Supporting Materials

One-step mechanochemical modification of biochar for enhanced Cd(II) removal

Ming Lei[1], Shixun Chen[1], Xiao Luo[1], Jin Zhang[1], Shuaima Wang[2], Daishe Wu[3], Zhifei Ma (✉)[1], Xiaori Wei[1], Bin Yang (✉)[4]

1 Key Laboratory of Poyang Lake Environment and Resource Utilization, Ministry of Education, School of Resources & Environment, Nanchang University, Nanchang 330031, China

2 Jiangxi Academy of Eco-Environmental Sciences and Planning, Nanchang 330077, China

3 School of Materials and Chemical Engineering, Pingxiang University, Pingxiang 337000, China

4 Technical Centre for Soil, Agriculture and Rural Ecology and Environment, Ministry of Ecology and Environment, Beijing 100012, China

✉ Corresponding authors

E-mail: groundwater308b@126.com (Z. Ma); qingyamu@126.com (B. Yang)

Text.S1. The chemicals involved in the research

The rice straw powder used in the experiment was collected from a rural area in Nanchang City, Jiangxi Province. The purity of all chemical reagents is AR grade. Among them, Na_2CO_3, $NaNO_3$, $CdCl_2$ and NaCl are from Shanghai Aladdin Technology Co., LTD., Na_2SO_4, NaF and KCl are from Xilong Science, and NaOH, $MgCl_2 \cdot 6H_2O$ and $CaCl_2$ are from Shanghai Sigma Technology Co., LTD, and all the chemicals are produced in China.

Text.S2. Detailed mechanochemical preparation of modified straw biochar

Sodium hydroxide and straw co-milled biochar (Al-bmST1), straw pre-activated with sodium hydroxide followed by ball milling (Al-bmST2), and straw directly ball-milled without chemical treatment (bmST) were all prepared using 100-mesh rice straw powder (denoted as ST), which was washed with deionized water and dried as the initial biomass raw material. The powder was then processed in a planetary ball mill. The specific methods are described as follows:

(1) In a 50 mL polytetrafluoroethylene (PTFE) ball mill jar, 10 zirconia balls with a diameter of 10 mm and 25 zirconia balls with a diameter of 6 mm were placed, along with 1 g of rice straw powder and 20 mL of sodium hydroxide solution at a specific concentration. After sealing the jar, it was loaded into a planetary ball mill and operated at a rotational speed of 500 r/min for 6 hours. The resulting biochar was thoroughly washed with deionized water until neutral pH was achieved, filtered, and then dried in an oven at 80℃ for at least 12 hours. Finally, the dried product was

ground into fine powder to obtain Al-bmST1.

(2) In another 50 mL PTFE ball mill jar, 1 g of rice straw powder, 10 zirconia balls (10 mm diameter), and 25 zirconia balls (6 mm diameter) were added. The jar was sealed and placed in the planetary ball mill under the same conditions: 500 r/min for 6 hours. After ball milling, the material was washed repeatedly with deionized water until neutral, filtered, and dried at 80℃ for at least 12 hours. The dried sample was then ground to obtain bmST.

(3) In a 50 mL beaker, 1 g of rice straw powder and 20 mL of sodium hydroxide solution of a specified concentration were mixed with a magnetic stirrer for 6 hours. The activated material was then washed with deionized water until neutral pH was reached, filtered, and dried at 80℃ for at least 12 hours. After drying, the sample was ground into powder. A 1 g portion of this powder was subjected to the same ball milling procedure as bmST to obtain Al-bmST2.

Text.S3. The characterization methods adopted in the research

The material characterization methods used in the research include Scanning Electron Microscope and Fourier Transform Infrared Spectrometer, X-Ray Diffraction, X-ray Photoelectron spectrometer and Specific Surface Area and Porosity Analyzer. Scanning electron microscopy (SEM) is used to characterize the microstructure characteristics of the material surface. Coupled with Energy Dispersive Spectrometer (EDS) technology, qualitative and quantitative analysis of the chemical composition in local areas can be achieved. The specific surface area and pore size analyzer (BET) is mainly used to determine the adsorption-desorption isotherm of porous materials, calculate the specific surface area based on Brunauer, Emmett and Teller theories, and analyze parameters such as pore size distribution and pore volume through the Barrett-Joyner-Halenda (BJH) model. Fourier Transform Infrared Spectrometer (FT-IR) characterizes the composition of functional groups, molecular structure and chemical bond features by analyzing the infrared absorption spectra of substances. X-ray photoelectron spectroscopy (XPS) characterizes the chemical states and composition distribution of elements on the surface of materials based on the photoelectron emission effect. X-ray diffraction (XRD) is based on the diffraction effect of crystals on X-rays and is used to analyze the crystal structure of materials.

Text.S4. Methods related to DFT calculation

All calculations were carried out with the Gaussian 16 software. Density functional theory (DFT) calculations were carried out with the B3LYP functional with the combination of the Grimme's D3BJ version of dispersion correction (Grimme et al., 2010). The basis set of 6-31G(d,p) for C, H, O and Lanl2dz for Cd were adopt for the geometry optimization and frequency calculation. The geometries were fully optimized without any structural constraints. The electrostatic potential visualized by Multiwfn software packages and VMD (Lu and Chen, 2012).

Text.S5. Life Cycle Assessment (LCA) Methodology

The environmental impacts were evaluated using SimaPro 9.5 software with the Ecoinvent 3.9.1 database, following the CML-IA baseline (v3.06) method. The functional unit (FU) was defined as the disposal and upcycling of 1 ton of raw rice straw. A "Cradle-to-Grave" system boundary was established, including pre-treatment (collection/transport), functional modification (one-step mechanochemistry vs. traditional pyrolysis), and environmental application (soil remediation). Mass-based allocation was utilized for co-products.

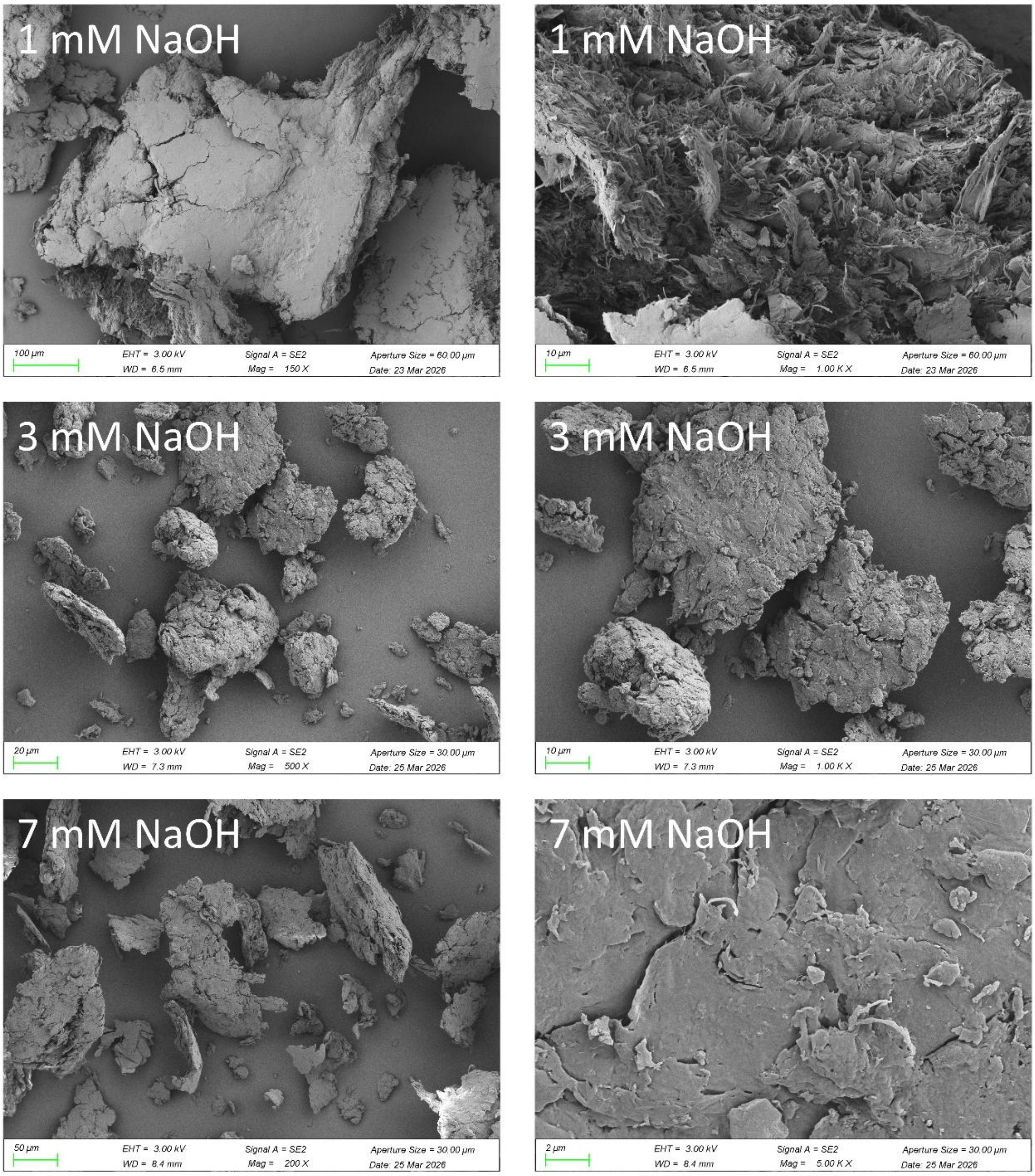

Figure.S1. SEM image of the adsorption materials obtained at different NaOH concentrations

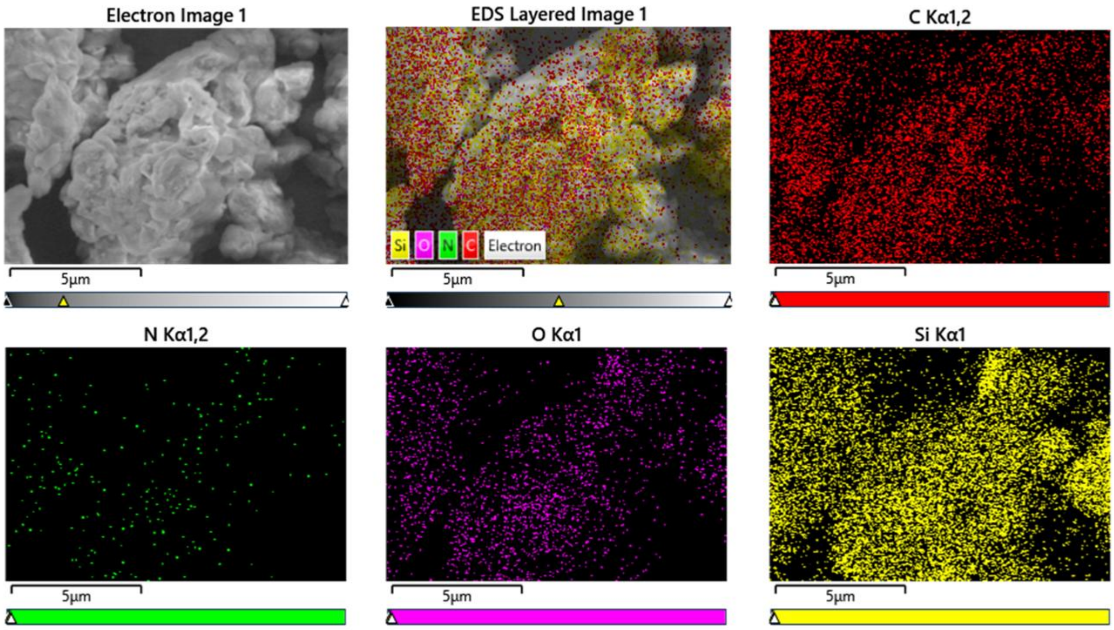

Figure.S2. SEM image of bmST

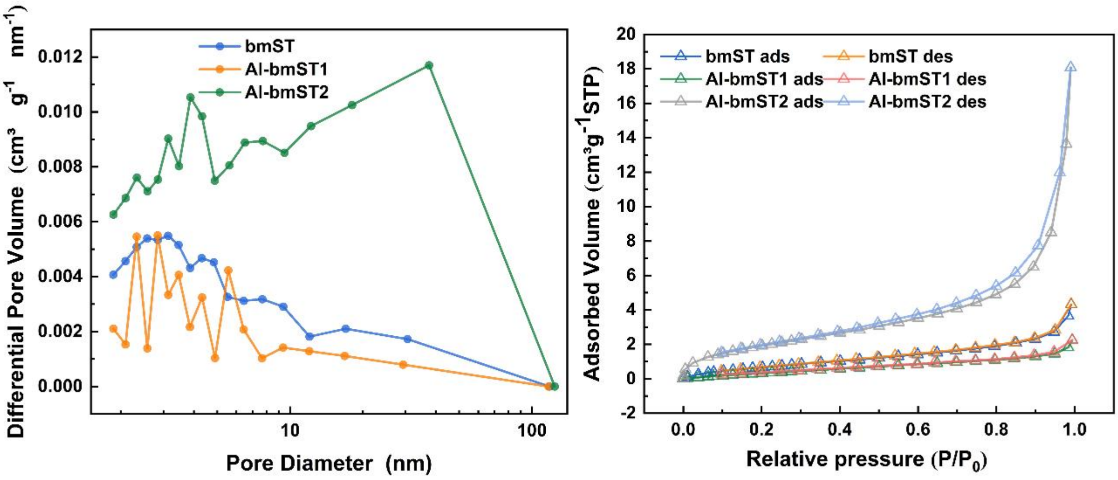

Figure.S3. N_2 adsorption-desorption isothermal curves and pore size distributions of bmST, Al-bmST1 and Al-bmST2

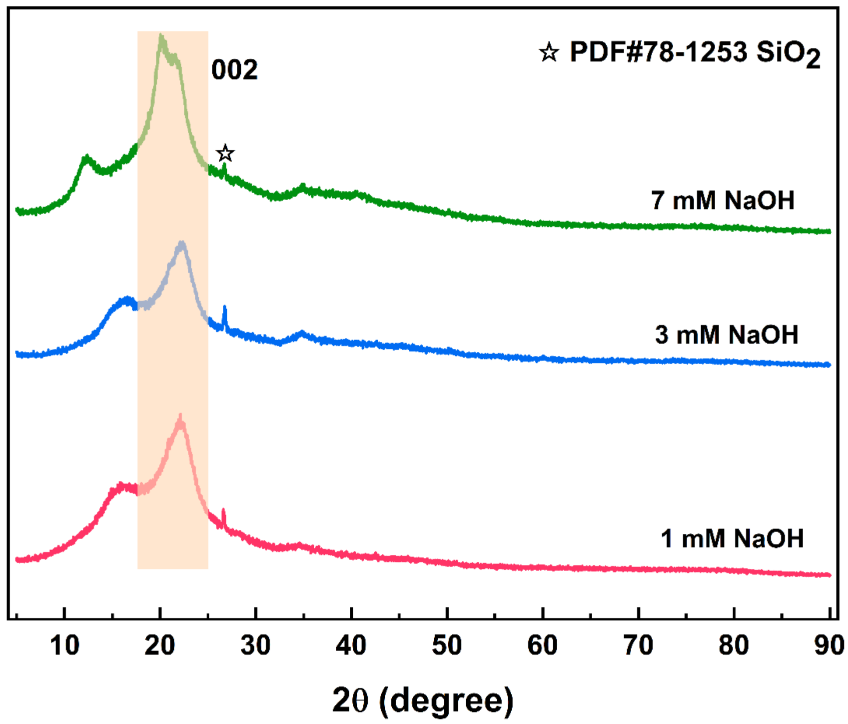

Figure.S4. XRD spectra of the adsorption materials obtained at different NaOH concentrations

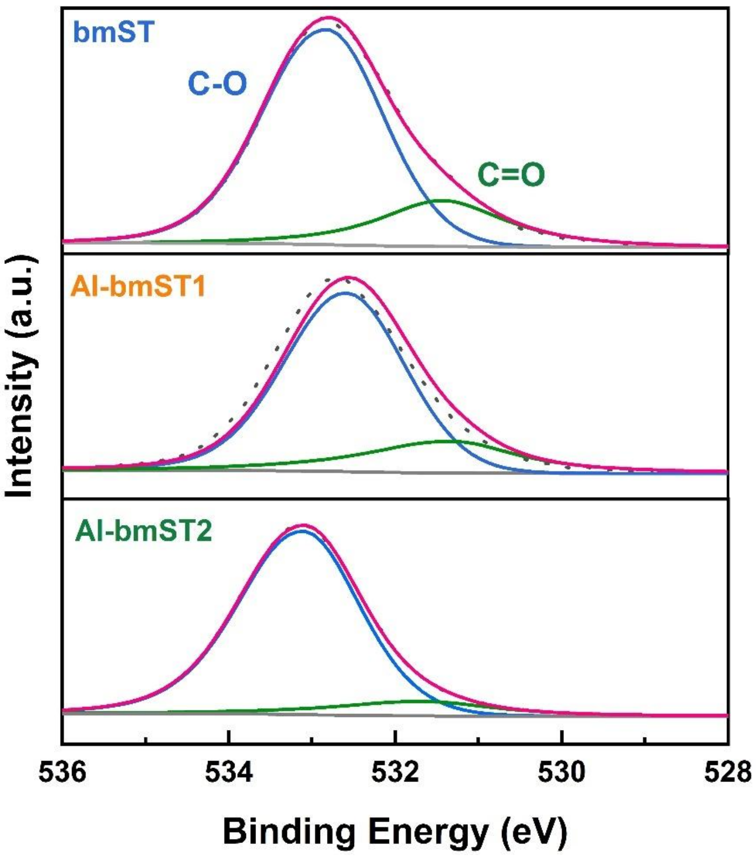

Figure.S5. Analysis of C1s energy spectra in XPS of bmST, Al-bmST1 and Al-bmST2

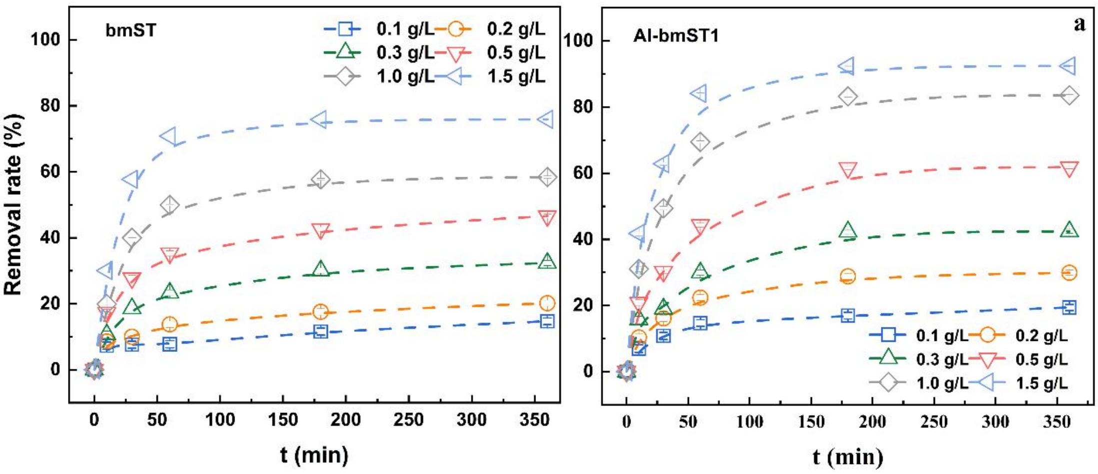

Figure.S6. The removal rate of Cd(II) by different dosages of bmST and Al-bmST1

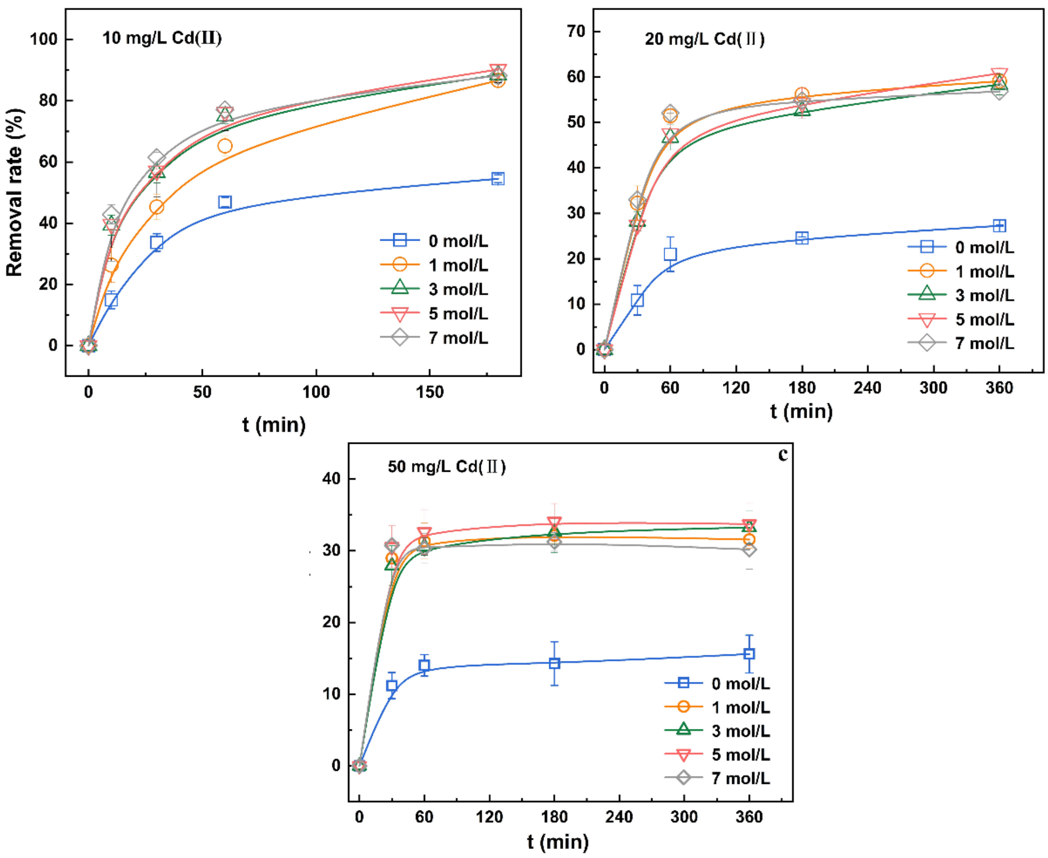

Figure.S7. Effect of Cd(Ⅱ) initial concentration on degradation of Al-bmST1

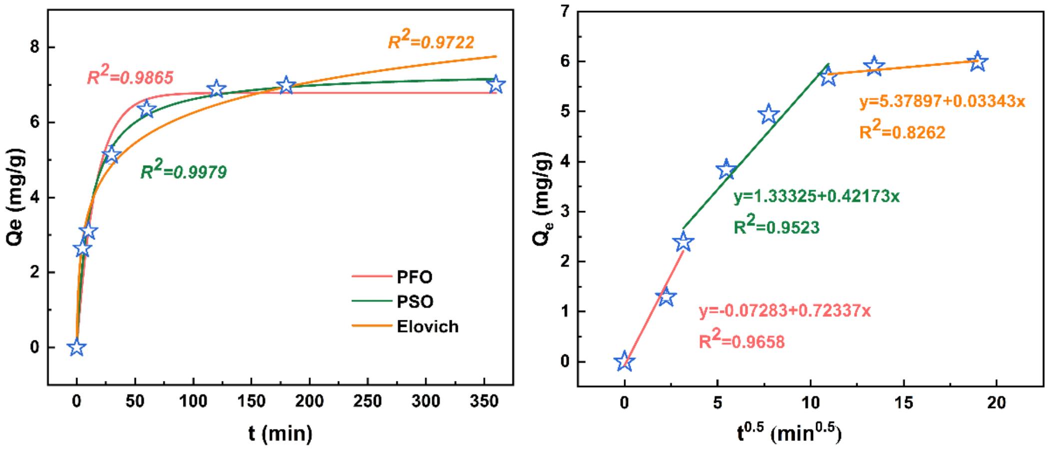

Figure.S8. The dynamic fitting and endogenous diffusion model of bmST

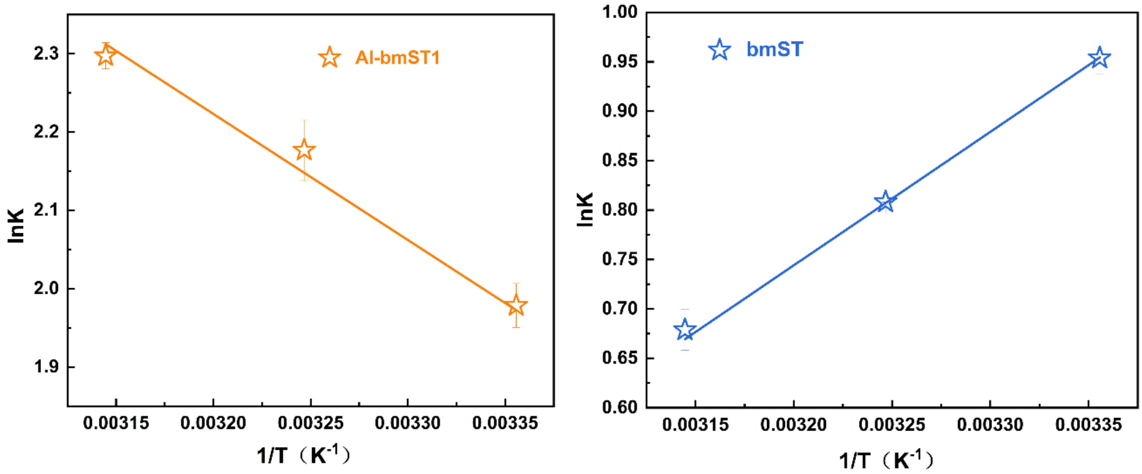

Figure.S9. Adsorption thermodynamics of bmST and Al-bmST1

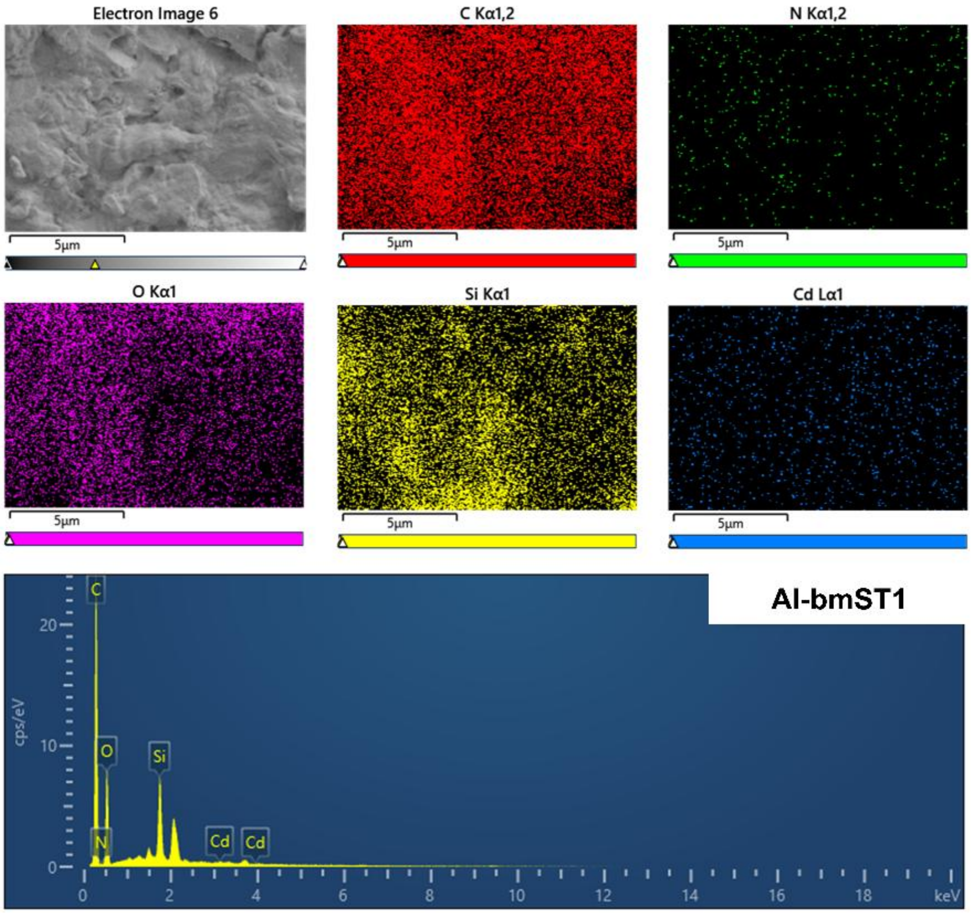

Figure.S10. SEM-EDS spectral scanning of Al-bmST1 after the reaction

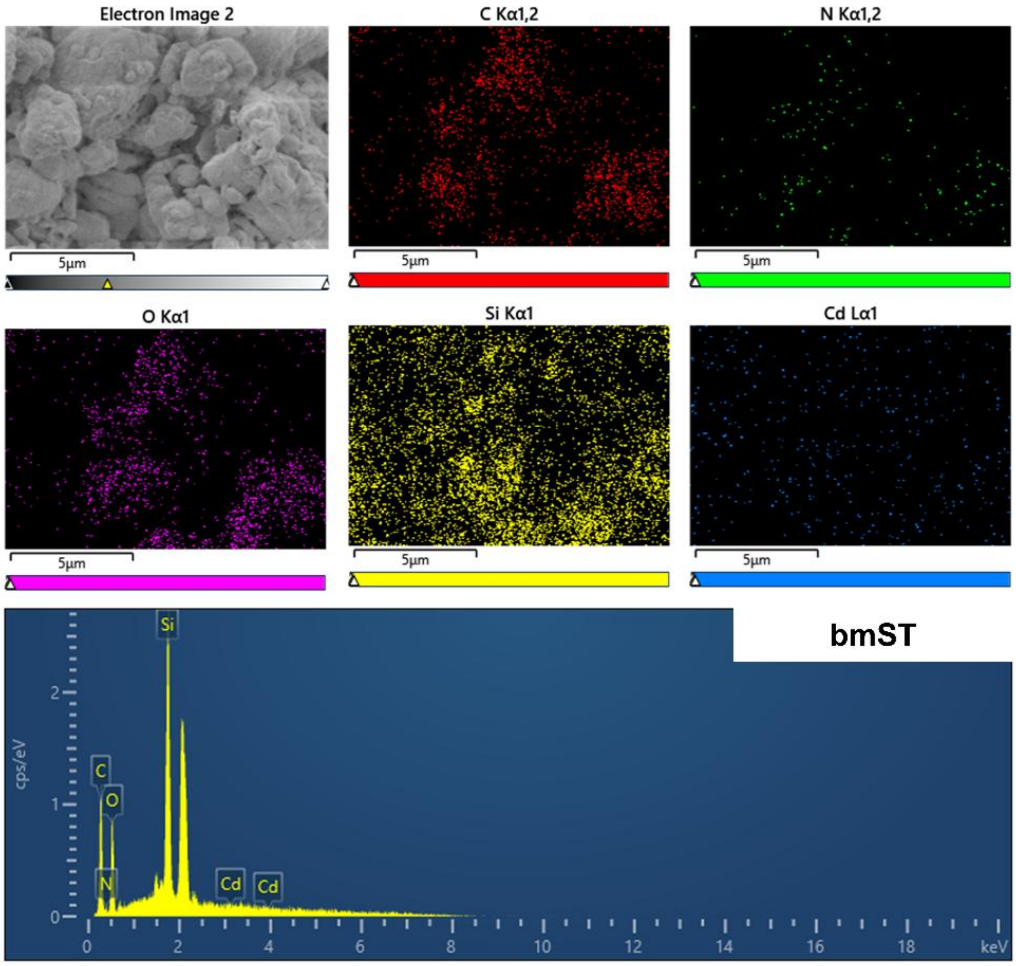

Figure.S11. SEM-EDS spectral scanning of bmST after the reaction

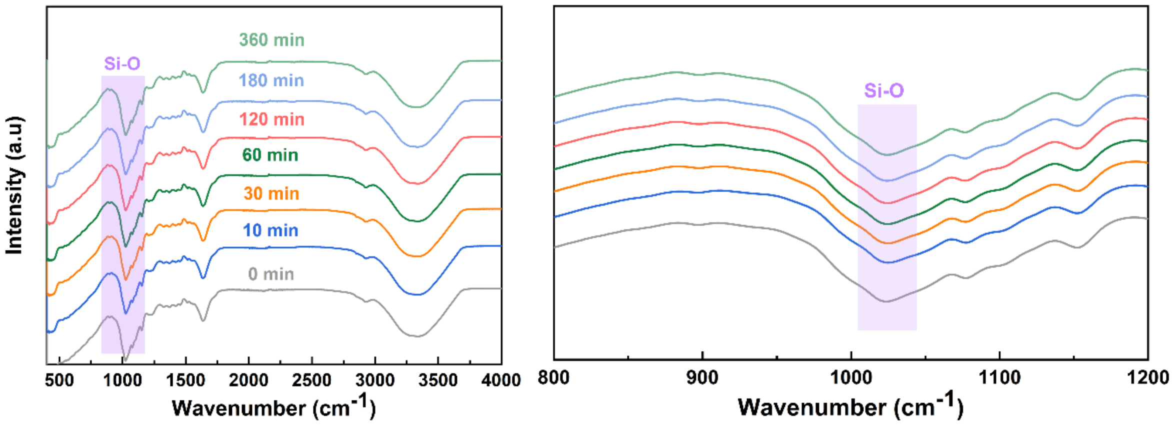

Figure.S12. In-situ infrared spectroscopy test diagram of bmST adsorbing Cd(II)

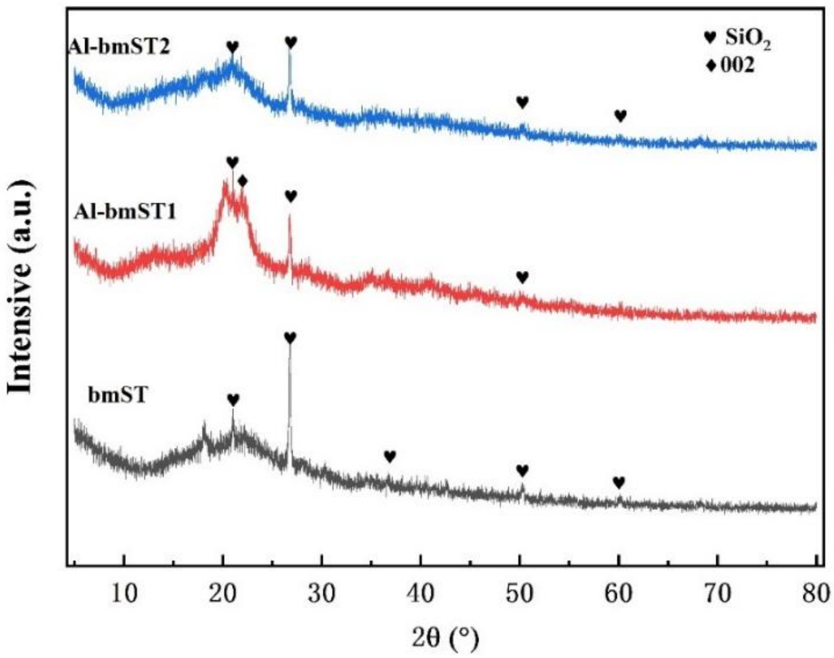

Figure.S13. Infrared spectrum after adsorption

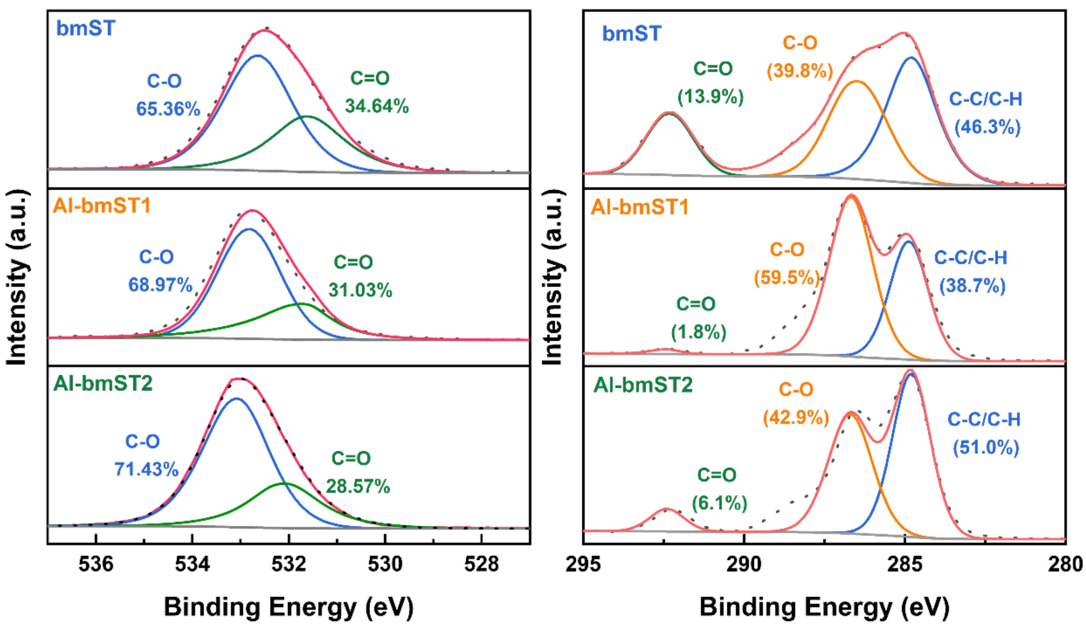

Figure.S14. XPS analysis of O1s and C1s spectra in bmST, Al-bmST1 and Al-bmST2 after adsorption

Table S1 BET specific surface area, total pore volume and average pore radius of bmST, Al-bmST1 and Al-bmST2

Sample	S_{BET} ($m^2 \cdot g^{-1}$)	V_{total} ($cm^3 \cdot g^{-1}$)	$D_{average}$ (nm)
bmST	3.0879	0.0065	8.4200
Al- bmST1	1.8873	0.0032	6.7822
Al- bmST2	7.4921	0.0277	14.7889

Table S2 XPS peak fitting data of bmST and Al-bmST1

Materials	Element	Component	Content (%)	Binding Energy (eV)	FWHM (eV)
bmST	C1s	O-C=O	16.67	292.35	1.32
		C-O-H	8.08	288.16	1.73
		C-O	24.75	286.65	1.45
		C-C/C-H	50.51	284.80	1.36
	O1s	C-O	80.00	532.82	1.67
		C=O	20.00	531.44	1.81
	N1s	Oxidized-N	10.43	406.01	0.78
		Graphitic-N	14.11	401.08	0.60
		Pyrrolic-N	61.35	400.11	1.30
		Pyridinic-N	14.11	398.92	1.56
	Si2p	SiO_2	32.55	104.78	1.49
		Silicate	47.17	103.64	1.42
		Si-O-C	20.28	102.36	1.42
AlbmST1	C1s	O-C=O	1.91	292.44	1.37
		C-O-H	7.18	288.45	1.62
		C-O	47.85	286.76	1.68
		C-C/C-H	43.06	284.80	1.56
	O1s	C-O	79.37	532.79	1.71
		C=O	20.63	531.49	1.82
	N1s	Oxidized-N	20.17	406.05	1.36
		Graphitic-N	5.15	401.56	0.50
		Pyrrolic-N	42.92	400.34	1.34
		Pyridinic-N	31.76	399.31	1.81
	Si2p	SiO_2	34.26	103.49	1.49
		Silicate	39.84	102.57	1.03
		Si-O-C	25.90	101.78	1.06

	C1s	O-C=O	7.69	292.20	1.38
		C-O-H	13.61	288.18	1.76
		C-O	59.17	286.62	1.58
		C-C/C-H	19.53	284.80	1.47
	O1s	C-O	90.09	533.01	1.67
		C=O	9.91	531.52	1.92
AlbmST2	N1s	Oxidized-N	29.29	407.00	1.18
		Graphitic-N	10.04	401.67	0.56
		Pyrrolic-N	41.84	400.29	1.35
		Pyridinic-N	18.83	398.86	1.51
	Si2p	SiO_2	48.54	103.68	1.33
		Silicate	16.02	102.85	1.16
		Si-O-C	35.44	101.74	1.18

Table S3 Adsorption kinetics fitting parameters for bmST and Al-bmST1

Equation	PFO		PSO		Elovich		
	K_1	R^2	K_2	R^2	α	β	R^2
bmST	0.04081	0.98652	0.00843	0.99786	0.81415	0.83008	0.97215
Al-bmST1	0.06122	0.97419	0.01171	0.99197	2.40194	0.85185	0.96651

Table S4 Parameters of intragranular diffusion model of bmST and Al-bmST1

Adsorption stage	Surface diffusion		Inter-particle diffusion		Particle internal diffusion	
	K_1	R^2	K_2	R^2	K_3	R^2
bmST	0.72337	0.96576	0.42173	0.95232	0.03343	0.8262
Al-bmST1	1.01835	0.97807	0.47534	0.88976	0.01314	0.7156

Table S5 Isothermal adsorption model fitting parameters of bmST and Al-bmST1 at normal temperature

Modle	Langmuir			Freundlich			Temkin		
	K_L	Q_m ($mg\cdot g^{-1}$)	R^2	K_F	1/n	R^2	K_T	A	R^2
bmST	0.24896	11.48463	0.98144	4.70373	0.21655	0.93952	5.93228	1.91885	0.96919
Al-bmST1	0.14176	27.05381	0.93002	6.08798	0.32353	0.99771	2.34644	5.02146	0.97796

Table S6 Comparison of adsorption properties of Cd (II) on various modified biochar

Material	Main elements	Preparation method	Q_m ($mg \cdot g^{-1}$)	References
Magnesium oxide loaded rice husk biochar	C, Mg	Pyrolysis	18.1	(Xiang et al., 2018)
Melamine-modified straw biochar	C, Fe	Pyrolysis	25.65	(Yin et al., 2024)
Composite modified sludge-based biochar	C, Mn	Pyrolysis	26.3	(Qian et al., 2025)
Waste mushroom substrate biochar	C	Pyrolysis	22.0	(Jiang et al., 2024)
Alkali-modified pecan biochar	C, Si	Pyrolysis, alkali soaking	0.98	(Ding et al., 2016)
FeC_2O_4-ball milled biochar	C, Fe	Pyrolysis, Ball-milling	2.78	(Pan et al., 2026)
Magnetic biochar	C, Fe	Complexation	7.03	(Liu et al., 2025)
Sawdust biochar	C	Pyrolysis	21.23	(Peng et al., 2017)
Fe/Mn Straw Biochar	C, Si, Fe, Mn	Pyrolysis	28.49	(Tan et al., 2022)
Soybean and purslane biochar	C	Pyrolysis	139.05	(Lian et al., 2020)
Straw biochar	C, Si	Pyrolysis	18.33	(Yan et al., 2022)
Modified corn stalks	C, Si	Chemical soaking	12.73	(Zheng et al., 2010)
Corn straw cellulose-based adsorbent	C, Si	Chemical soaking	47.07	(Lai et al., 2020)
Coconut shell biochar	C, Si	-	44.80	(Paranavithana et al., 2016)

$KMnO_4$ modified coconut shell biochar	C, Si, Mn	Chemical soaking	16.33	(Bian et al., 2024)

Table S7 Adsorption thermodynamic model parameters of bmST and Al-bmST1

Material	T (K)	ΔG ($kJ\ mol^{-1}$)	ΔH ($kJ\ mol^{-1}$)	ΔS ($J\ mol^{-1}\ K^{-1}$)	R^2
bmST	298	-2.363	-11.228	-29.743	0.999
	308	-2.070			
	318	-1.768			
Al-bmST1	298	-4.852	13.385	61.317	0.979
	308	-5.574			
	318	-6.074			

Table S8 The input list for the entire life cycle assessment process

Stage	Input	Unit	Traditional Pyrolysis	One-step Mechanochemical
Pre-treatment	Rice straw	t	1.0	1.0
	Transport	km	100	100
	Electricity	kWh	14.25	14.25
Modification	Electricity	kWh	428	205
	NaOH	kg	-	300
	Water	kg	-	5000
	Brick	kg	0.1	0.1
Soil remediation	Biochar	t	0.6	0.6
	Poultry manure	t	0.1	0.1
	Electricity	kWh	19.5	19.5

Table S9 The output list for the entire life cycle assessment process

Stage	Output	Unit	Traditional Pyrolysis	One-step Mechanochemical
Pre-treatment	CO_2 Emission	kg	8.5	8.5
Modification	CO_2	kg	110	20
	CH_4	kg	0.8	-
	NO_x	kg	1.2	-
	Dioxin	Ng TEQ/m^3	0.05	-
	PM	kg	22	5
	Bio-oil	t	0.29 (offset 30% of the electricity)	-
Soil remediation	CO_2 Emission	kg	5	3
	CH_4	kg	0.09	0.09
	N_2O	kg	0.012	0.012
	NH_3	kg	0.24	0.24
	Treat heavy metal-contaminated soil	t	75	-

References

Bian Y, Zhang F, Liu Q, Mo X, Xu T, Yi W, Xu Y, Bai S, Liu L (2024). Simultaneous removal capacity and selectivity of Cd(II) and Ni(II) by KMnO4 modified coconut shell and peach kernel biochars. Journal of Water Process Engineering, 65: 105862

Ding Z, Hu X, Wan Y, Wang S, Gao B (2016). Removal of lead, copper, cadmium, zinc, and nickel from aqueous solutions by alkali-modified biochar: Batch and column tests. Journal of Industrial and Engineering Chemistry, 33: 239-245

Grimme S, Antony J, Ehrlich S, Krieg H (2010). A consistent and accurate ab initio parametrization of density functional dispersion correction (DFT-D) for the 94 elements H-Pu. The Journal of Chemical Physics, 132(15): 154104

Jiang C, Huang S, Jiang Y, Li Y, Miao T, Jin Y, Qu J, Liu X, Wang W (2024). Effects of aging processes on spent mushroom Substrate-Derived Biochar: Adsorption characteristics of Cd(II) and Cr(VI). Arabian Journal of Chemistry, 17(9)

Lai C, Huang F, Wu Y, Wang R (2020). Reasonable design of a corn stalk cellulose-based adsorbent for adsorption of Cd(II) and Ni(II): adsorption behaviors and mechanisms. Desalination and Water Treatment, 202: 327-344

Lian W, Yang L, Joseph S, Shi W, Bian R, Zheng J, Li L, Shan S, Pan G (2020). Utilization of biochar produced from invasive plant species to efficiently adsorb Cd (II) and Pb (II). Bioresource Technology, 317: 124011

Liu N, Zhou R, Huang S, Zhang J, Zhang H, Liu H, Du X, Zhang D, Zhang R, Sun Z, Fu S, Zhan X (2025). Effects of ferrite porous confined biochar nanoreactor on the adsorption and desorption of Pb and Cd. Journal of Water Process Engineering, 74: 107717

Lu T, Chen F (2012). Multiwfn: A multifunctional wavefunction analyzer. Journal of Computational Chemistry, 33(5): 580-592

Pan S, Huang Y, Zhou W, Ge F, Zhu L (2026). FeC2O4-ball milled biochar for simultaneous removal of cadmium and tetracycline: A strategy coupling oxygen vacancies with carboxyl groups. Colloids and Surfaces A: Physicochemical and Engineering Aspects, 738: 139999

Paranavithana G N, Kawamoto K, Inoue Y, Saito T, Vithanage M, Kalpage C S, Herath G B B (2016). Adsorption of Cd2+ and Pb2+ onto coconut shell biochar and biochar-mixed soil. Environmental Earth Sciences, 75(6): 484

Peng H, Gao P, Chu G, Pan B, Peng J, Xing B (2017). Enhanced adsorption of Cu(II) and Cd(II) by phosphoric acid-modified biochars. Environmental Pollution, 229: 846-853

Qian J, Cai Q, Zheng T, Wu J, Sun F, He R, Kamran M A, Zhan J, Huang X (2025). Competitive and synergistic effects of biochar modified with phosphoric acid and manganese oxide on the removal of Cd and Congo red from wastewater. Journal of Water Process Engineering, 69

Tan W-T, Zhou H, Tang S-F, Zeng P, Gu J-F, Liao B-H (2022). Enhancing Cd(II) adsorption on rice straw biochar by modification of iron and manganese oxides. Environmental Pollution, 300: 118899

Xiang J, Lin Q, Cheng S, Guo J, Yao X, Liu Q, Yin G, Liu D (2018). Enhanced adsorption of Cd(II) from aqueous solution by a magnesium oxide-rice husk biochar composite. Environ Sci Pollut Res Int, 25(14): 14032-14042

Yan S, Yu W, Yang T, Li Q, Guo J (2022). The Adsorption of Corn Stalk Biochar for Pb and Cd: Preparation, Characterization, and Batch Adsorption Study, 22

Yin Z-X, Zhang Y-Y, Liu J-X, Huang F, Liu Q-J, Huang M-Z, Xiao R-B, Gao G-Y, Lan T-Z, Zhou X (2024). Quantitative mechanisms for the Cd2+ adsorption increased by sewage-sludge biochar but decreased by rice-straw biochar after melamine modification. Journal of Environmental Chemical Engineering, 12(6)

Zheng L, Dang Z, Yi X, Zhang H (2010). Equilibrium and kinetic studies of adsorption of Cd(II) from aqueous solution using modified corn stalk. Journal of Hazardous Materials, 176(1): 650-656